

Chemistry in Cosmic-Ray Dominated Regions (CRDRs)

E. Bayet^{1*}; D.A. Williams¹; T. W. Hartquist² and S. Viti¹

¹*Department of Physics and Astronomy, University College London, Gower Street, London WC1E 6BT, UK*

²*School of Physics and Astronomy, University of Leeds, Leeds LS2 9JT, UK*

Accepted ; Received ; in original form

ABSTRACT

Molecular line observations may serve as diagnostics of the degree to which the number density of cosmic ray protons, having energies of 10s to 100s of MeVs each, is enhanced in starburst galaxies and galaxies with active nuclei. Results, obtained with the UCL_PDR code, for the fractional abundances of molecules as functions of the cosmic-ray induced ionisation rate, ζ , are presented. The aim is not to model any particular external galaxies. Rather, it is to identify characteristics of the dependencies of molecular abundances on ζ , in part to enable the development of suitable observational programmes for cosmic ray dominated regions (CRDRs) which will then stimulate detailed modelling. For a number density of hydrogen nuclei of of 10^4 cm^{-3} , and high visual extinction, the fractional abundances of some species increase as ζ increases to 10^{-14} s^{-1} , but for much higher values of ζ the fractional abundances of all molecular species are significantly below their peak values. We show in particular that OH, H₂O, H₃⁺, H₃O⁺ and OH⁺ attain large fractional abundances ($\geq 10^{-8}$) for ζ as large as 10^{-12} s^{-1} . HCO⁺ is a poor tracer of CRDRs when $\zeta > 10^{-13} \text{ s}^{-1}$. Sulphur-bearing species may be useful tracers of CRDRs gas in which $\zeta \sim 10^{-16} \text{ s}^{-1}$. Ammonia has a large fractional abundance for $\zeta \leq 10^{-16} \text{ s}^{-1}$ and nitrogen appears in CN-bearing species at significant levels as ζ increases, even up to $\sim 10^{-14} \text{ s}^{-1}$. In this paper, we also discuss our model predictions, comparing them to recent detections in both galactic and extragalactic sources. We show that they agree well, to a first approximation, with the observational constraints.

Key words: Submillimeter: general – Galaxies: star formation – Galaxies: ISM – ISM: abundances – Methods: numerical – Astrochemistry

1 INTRODUCTION

The high spatial density of massive star formation in mergers and starburst galaxies (e.g. Acero et al. 2009; Suchkov et al. 1993; Acciari et al. 2009) creates regions of extremely high cosmic ray energy density, up to about ten thousand times that in the Milky Way Galaxy. Papadopoulos (2010) has proposed that these large energy densities alter the heating rates and ionization fractions in dense gas ($n(\text{H}_2) \gtrsim 1 \times 10^4 \text{ cm}^{-3}$) in the UV-shielded cores that contain much of the molecular gas in these galaxies, so that these cosmic ray-dominated regions (CRDRs) have different initial conditions for star formation (Papadopoulos 2010; Papadopoulos et al. 2010). These conditions affect the subsequent evolution of the gas and may even lead to a top-heavy Initial Mass Function and bimodal star formation (Papadopoulos et al. 2010).

It is therefore important to determine whether there

may be useful molecular tracers of CRDRs. Papadopoulos (2010) has suggested several possible chemical signatures, but it seems necessary to make a fairly complete and self-consistent thermal/chemical model of dense gas subjected to very high fluxes of cosmic rays. Historically, the cosmic ray ionization rate in Galactic diffuse and molecular clouds has normally been determined by treating it as a free parameter and matching the predicted chemistry to that observed (e.g. Black & Dalgarno 1977; Hartquist et al. 1978a and Hartquist et al. 1978b). Here, it is necessary to reverse that procedure and to compute the variation of the chemistry as the ionization rate is increased. Lepp & Tiné (1998) made such a calculation and computed the chemistry in dense gas subjected to ionization rates varying over a wide range. However, their calculation was for a fixed temperature. Later, Meijerink & Spaans (2005), Spaans & Meijerink (2005), and Meijerink et al. (2006) concentrated on a restricted chemical network with enhanced ionization rate. Recently, Bayet et al. (2009) compared the computed chemistry for a large network of 131 species connected in 1700

* E-mail: eb@star.ucl.ac.uk; daw@star.ucl.ac.uk;
twh@ast.leeds.ac.uk; sv@star.ucl.ac.uk

reactions at just two particular cosmic ray ionization rates (the canonical Milky Way value and 100 times this value) in a self-consistent thermal/chemical and time-dependent one-dimensional model. In the present work, we use the same model as that of Bayet et al. (2009) and compute the chemistry for many ionization rates from Milky Way values up to about one million times larger.

The thermal/chemical model is described in Section 2, and the input parameters are discussed in Section 3. The outputs of the computations are the temperature and the chemical abundances as functions of visual extinction (from $A_v = 3$ to 20 magnitudes) and of the cosmic ray ionisation rate (from $\zeta = 2 \times 10^{-17} \text{ s}^{-1}$ to $\zeta = 5 \times 10^{-11} \text{ s}^{-1}$). The model outputs are presented in Section 4. The relevance of our modelling to observations of galaxies is considered in Section 5, where we also give our conclusions.

2 MODEL DESCRIPTION

The model used for our study of the chemistry in CRDRs is the UCL_PDR model as described in Bell et al. (2005, 2006). This is a time-dependent Photon-Dominated Region (PDR) model with constant density. In the present application, the code is run for 10^8 yrs by which time chemical steady state is reached in all models. Checks that we have made confirm that the fractional abundances at 10^6 yrs do not differ significantly from those at 10^8 yrs. However, even for high values of ζ , the chemistry requires close to 10^6 yrs to approach steady state. Though the timescale to convert atomic carbon to CO decreases with increasing ζ , neutral-neutral reactions limit the rates at which many of the observable species form. Those rates do not depend sensitively on ζ for values in excess of about 10^{-17} s^{-1} . However, they do decrease with decreasing metallicity.

The code operates in one space dimension for an assumed semi-infinite slab geometry, and computes self-consistently the chemistry and the temperature as functions of depth and time within a semi-infinite slab, taking account of a wide range of heating and cooling processes. In the present work, the code is used to determine the chemical and thermal properties at all depths up to 20 visual magnitudes. For the present work, and consistent with the Bayet et al. (2010) version of the code, additional radiative cooling due to rotational transitions of ^{13}CO , C^{18}O , CS, OH and H_2O have been implemented. The escape probability formalism of de Jong et al. (1980) is used to determine non-LTE level populations and resulting line intensities at each depth- and time-step, in the same manner as for the existing coolants in the code. Collisional rates with H_2 are taken from the Leiden Atomic and Molecular Database (LAMDA; Schöier et al. 2005). The inclusion of these coolants allows the thermal balance to be more accurately determined in warm dense gas at high extinction. The UCL_PDR code also includes cooling due to the OI metastable levels, and the O - H^+ collisions and O - e^- collisions which excite them; these are important for the models for high values of ζ . The treatment of H_2 self-shielding has also been updated to use the results of detailed calculations performed by Lee et al. (1996), as described in Bayet et al. (2010). The chemical network links 131 species in over 1834 gas-phase reactions; only H_2 is formed by surface chemistry; freeze-out

of species on to grain surfaces is excluded. The UCL_PDR code has been validated against all other commonly used PDR codes (Röllig et al. 2007).

The model should be appropriate for regions with temperatures up to several thousand degrees. However, it is not valid for regions with temperatures approaching 10^4 K and the associated high fractional ionisations. Thus, we present results only for models for which ζ is 10^{-12} s^{-1} or less. Codes such as MOCASSIN (Ercolano et al. 2005) or CLOUDY (Ferland et al. 1998) might be more suitable for models with higher values of ζ . The model does not include doubly ionised species other than Ca^{++} , though cosmic-ray induced ionisation will produce a variety of them (see Shaw et al. 2008). Charge transfer with neutral hydrogen atoms will contribute substantially to the removal of many of them in regions with ζ ranging from 10^{-14} to 10^{-12} s^{-1} .

3 PARAMETER SELECTION

The model requires the setting of a number of physical and chemical parameters. The choices we have made are listed in Table 1. We comment here on some of these. All the calculations are made for an assumed gas number density of 1×10^4 hydrogen nuclei (in all forms) cm^{-3} .

The cosmic ray ionisation rate is a free parameter in these calculations, and allowed to take values that range from $\zeta = 2 \times 10^{-17} \text{ s}^{-1}$ to $1 \times 10^{-12} \text{ s}^{-1}$.

The lowest value of ζ selected here is comparable to that inferred for the Milky Way, while the highest value of ζ is comparable to the highest values suggested to be appropriate for compact extragalactic starburst regions (cf. eqn. 6 of Papadopoulos 2010).

Galaxies are observed to have a range of metallicities (e.g. Bayet et al. 2006, Bell et al. 2006); we have considered a range from 0.1 to 4 times solar metallicity. Most of our computations are made using metallicity of 0.1 times solar, a value that may represent conditions in fairly young galaxies. However measurements of metallicity in some galaxies show both near-solar and larger than solar values (NGC 253, M 82, IC 342 - see e.g. Zaritsky et al. 1994), so we have also made calculations with higher metallicities.

Several other parameters are assumed to scale linearly with metallicity. These are the dust:gas mass ratio, the H_2 formation rate, and the initial elemental abundances. The values of these parameters for solar metallicity are given in Table 1. The elemental abundances given there are derived from Sembach & Savage (1996); Sofia et al. (1997); Meyer et al. (1998); Snow et al. (2002); and Knauth et al. (2003).

The models require the specification of the mean dust grain radius and albedo, which affect the transfer of external radiation into the cloud. The values given in Table 1 are canonical. The external radiation field impinging on the one-dimensional semi-infinite slab is assumed to be 1000 Habing, much larger than for the Milky Way but possibly appropriate for regions of active star formation in which CRDRs may be located. This value is comparable to values obtained from molecular line intensity modelling for several galaxies (e.g. Bayet et al. 2006 and Aalto 2008). The chemistry in the one-dimensional semi-infinite slab is explored as a function of depth or visual extinction, A_v , from the edge ($A_v = 0$) up

to $A_v = 20$ mag. The model also requires for line-width calculations the specification of the microturbulence velocity. We use the value adopted by Bayet et al. (2009).

4 RESULTS

We present in Fig 1-4 results for the temperature and chemistry at the three representative depths into the one-dimensional slab: $A_v = 3, 8$ and 20 mag.

The case $A_v = 3$ is intended to represent translucent material, $A_v = 8$ to represent the extended PDR gas (as detected in the nuclei of M82, NGC 253, IC 342 and NGC 4038 by Bayet et al. 2009), while $A_v = 20$ represents dense PDR components detected in galaxies (Bayet et al. 2008).

Fig. 1 shows the results for temperature obtained from the self-consistent thermal balance, as a function of cosmic ray ionisation rate, at these three values of A_v . All three curves show the same general behaviour, rising from low values at low ionisation rates to temperatures approaching 1×10^4 K for the highest ionisation rates. As will be evident in the plots of the chemical abundances, reactions at these very high temperatures destroy much of the chemistry. There is some difference in temperature between the three curves shown for low values of the ionisation rate. At $A_v = 3$ mag, the temperature lies between 50 and 100 K for ionisation rates less than about $1 \times 10^{-14} \text{ s}^{-1}$. This relatively high temperature is maintained by the intense external radiation field. However at $A_v = 8$ mag, the temperature falls to ~ 10 K at the lowest ionisation rates, as expected, since the external radiation field no longer plays a role.

We note that the models give slightly higher temperatures at $A_v = 20$ mag than at $A_v = 8$ mag. This is due to the fact that at high visual extinctions the C and CO lines become optically thick and hence are less able to cool the gas whilst the cosmic ray heating remains high and constant. For some models, there were some small difficulties associated with the convergence of the thermal balance. For example one sees small spikes in the thermal structure curve for $A_v = 3$ and corresponding features in the plots of the fractional abundances. These difficulties are not due to bistability (Boger & Sternberg 2006). Rather they arise due to the stiffness of the coupled chemical and thermal balance equations. Their influence on the calculated abundances of observable species is not significant. The effects of high heating rates on the chemistry is further investigated in Bayet et al. (2010).

Fig. 2, 3 and 4 present the results giving the abundances of various relevant species at the three specified values of A_v . These species were selected from the 131 available partly because many of them have already been detected in external galaxies, and partly to illustrate the sensitivity of species to the ionisation rate for a wide chemical variety. The range of abundances shown extends somewhat beyond the values that may be detectable.

Although there are significant differences, the three cases are broadly similar in their behaviour with respect to the enhancement of the ionisation rate. As the ionisation rate is increased from a value appropriate for the Milky Way, a rich chemistry is maintained up to a critical value of the ionisation rate, beyond which the molecular abundances fall rapidly as the ionisation rate is further increased. If the

ionisation rate is increased to $1 \times 10^{-12} \text{ s}^{-1}$, almost all the chemistry is effectively suppressed. The driver of this decline in molecular abundances is linked to the decline in molecular hydrogen; this occurs when the ionisation rate is about $1 \times 10^{-14} \text{ s}^{-1}$, and H_2 becomes a minor species when the ionisation rate is as large as 10^{-12} s^{-1} . In these conditions, conventional astrochemistry - based on reactions with H_2 molecules - ceases. In this range of ionisation rate, the temperature rises abruptly to some thousands of Kelvin (see Fig. 1), and hot atomic hydrogen is very destructive of molecules. However, we can see from the figures that potential molecular tracers can be identified for ionisation rates of about $1 \times 10^{-13} \text{ s}^{-1}$ but the molecular abundances drop substantially as ζ increases much more.

We now confine our remarks to the chemically richer regions of parameter space. There are some differences between the panels in Fig. 3 (or 4). Some species decline with increasing ionisation rate more rapidly than others. For example, sulphur-bearing species may be useful tracers of gas in which $\zeta = 10^{-16} \text{ s}^{-1}$ but not when $\zeta = 10^{-14} \text{ s}^{-1}$. Ammonia has a large fractional abundance for lower ionisation rates, but the abundance declines rapidly as the ionisation rate increases. Nitrogen appears in CN-bearing species at levels that are probably significant as the ionisation rate increases, even up to $\sim 10^{-14} \text{ s}^{-1}$.

There are some differences between the figures shown. At $A_v = 3$, molecular abundances are significantly lower than those for higher visual extinctions. For example, CS is $\sim 10^4$ times more abundant at $A_v = 8$ than at $A_v = 3$. The intense radiation field assumed in these models to impinge on the slab is responsible for inhibiting the chemistry at $A_v = 3$. However, the model results for $A_v = 8$ and 20 magnitudes are essentially identical, as the external radiation field does not penetrate effectively to these depths.

The behaviour of oxygen and carbon hydrides and their ions is somewhat different to the above behaviours. Some of these species show fractional abundances of rather high levels for ionisation rates of 10^{-14} s^{-1} , while others even sustain these high values for ionisation rates approaching $\sim 10^{-12} \text{ s}^{-1}$. For example, OH and H_2O fractional abundances are $\sim 10^{-7}$ for an ionisation rate of $\sim 10^{-14} \text{ s}^{-1}$, while OH and OH^+ may be as large as $\sim 10^{-8}$ even for an ionisation rate of $\sim 10^{-12} \text{ s}^{-1}$. The ions H_3^+ and H_3O^+ are likely to be abundant for $\zeta = 10^{-13} \text{ s}^{-1}$; however, the commonly used tracer HCO^+ is probably useless for values of ζ larger than 10^{-13} s^{-1} . The behaviour of these oxygen and carbon species is a consequence of the thermal stimulation of the endothermic reactions that may initiate oxygen and carbon chemistry by the increase in kinetic temperature arising from the higher ionisation rates. However, ultimately, the reduction in the H_2 fraction suppresses these reaction networks.

Given that the metallicity in some galaxies has been measured (see Section 5) and the values found to lie in a range often below but sometimes exceeding the solar value, it is worthwhile to explore the predictions of molecular abundances in our model for varying metallicity. Table 2 shows the computed fractional abundances for some atoms and molecules of observational interest for three values of the metallicity (0.1, 1.0 and 4.0 times the solar value), for both ‘‘high’’ (10^{-13} s^{-1}) and ‘‘low’’ (10^{-16} s^{-1}) cosmic ray ionisation rates, and for two values of the visual extinction ($A_v = 3$ and 20 magnitudes). The results for the case when $A_v =$

8 mag are closely similar to those for $A_v = 20$ mag, and are not shown. The “high” ionisation rate is intended to represent the case predicted by Papadopoulos (2010) for CRDRs, while the “low” case is expected to be roughly appropriate for galaxies similar to the Milky Way.

As has been found by earlier studies of the dependence of chemistry on the metallicity, the behaviour is rather complicated. At first sight one may expect a higher metallicity to lead to larger fractional abundances of molecules. However, because of the chemical rate equations are strongly coupled, some species tend to increase with metallicity, while others decrease, for a given ionisation rate. Further, Table 2 shows that different behaviours may occur when the ionisation rate is changed. For example, the fractional abundance of C_2H at $A_v = 3$ mag with a high ionisation rate is a strongly increasing function of metallicity, while for $A_v = 20$ mag and a low ionisation rate the C_2H fractional abundance declines rapidly with increasing metallicity.

CO is generally fairly strongly dependent on metallicity as it is formed in successive reactions. However, at $A_v = 3$ mag with a low metallicity, the molecule does not attain an abundance high enough to provide self-shielding against the radiation field which destroys this molecule through line absorption. Thus, at low metallicity, the fractional abundance of CO is also low for $A_v = 3$ mag. Consequently, HCO^+ is similarly affected.

These kinds of behaviour can be understood in terms of the rates of the various competing processes. At $A_v = 3$ mag, the intense radiation field adopted in these calculations (1000 Habing) may lead to photodissociation being a competitive process with ion-molecule reactions, while at higher values of A_v photodissociation is negligible. The ionisation rate drives the chemistry when photo-processes do not play a role, and high ionisation rates drive the chemistry much faster than low rates. Thus, in the case of C_2H , the dependence on metallicity is strong because it is formed by successive reactions involving C^+ , itself dependent on metallicity. Thus, at $A_v = 3$ mag both photons and high fluxes of cosmic rays drive the chemistry strongly to create large abundances at high metallicities. However, at $A_v = 20$ mag with low ionisation rates, the C^+ and C_2H abundances never attain high values, even at the highest metallicity. It is evident, therefore, that the choice of potential tracers depends sensitively on ionisation rate as well as metallicity.

5 DISCUSSION AND CONCLUSIONS

In this section we briefly explore the relevance of our theoretical predictions for galactic and extragalactic environments. We remind the reader that our attempt in this paper is not to model any particular source but rather to indicate qualitatively if our model predictions (i.e. the variations of the species fractional abundances with respect to the changes in cosmic ray ionisation rate) agree to a first approximation with observations in the local and nearby Universe.

Recent results indicate that higher cosmic ray ionization rates might be present in diffuse clouds throughout the Galaxy and in the Orion bar (e.g. Indriolo et al. 2007; Shaw et al. 2008; Indriolo et al. 2009 and even more recent results from Herschel/HIFI such as Gupta et al. 2010; Neufeld et al. 2010). More precisely, Indriolo et al. (2007)

presents H_3^+ column densities varying between $0.2-2.1 \times 10^{14} \text{ cm}^{-2}$ depending on the diffuse cloud observed (see their Tables 3 and 4). They derive estimates of $\zeta \sim 0.5 - 3.2 \times 10^{-16} \text{ s}^{-1}$. If we convert these column densities into fractional abundance estimates (i.e. $4.4 \times 10^{-9} - 4.4 \times 10^{-8}$) and compare them with those provided by our model showing the smallest A_v (i.e. Fig. 2 for $A_v = 3$ mag) and $\zeta = 2 \times 10^{-16} \text{ s}^{-1}$, we find a very good agreement. Despite this encouraging agreement, the interpretation of the H_3^+ observations is a highly debated subject and a more detailed analysis, requiring the modelling of a particular set of galactic sources (outside the scope of this paper) is required for any definitive conclusions. Indriolo et al. (2009) invoke a low-energy (~ 10 MeV) cosmic ray flux for a plausible explanation for the observed H_3^+ results. Chemical models such as ours cannot be used to infer details of the cosmic ray spectrum responsible for inducing the ionization.

Towards W49N, Neufeld et al. (2010) estimated column densities of OH^+ varying between $2.2 \times 10^{13} \text{ cm}^{-2}$ and $2.6 \times 10^{14} \text{ cm}^{-2}$ whereas column densities of H_2O^+ range from $4.2 \times 10^{12} \text{ cm}^{-2}$ to $2.7 \times 10^{13} \text{ cm}^{-2}$. These authors also inferred that these species are located in clouds of low molecular fraction. From their column densities we derive fractional abundances estimates of OH^+ of about $4.5 \times 10^{-9} - 5.4 \times 10^{-8}$ and for H_2O^+ of about $8.8 \times 10^{-10} - 5.6 \times 10^{-9}$. OH^+ fractional abundances are in agreement with our models having $\zeta > 5 \times 10^{-14} \text{ s}^{-1}$ (see Fig. 2) whereas H_2O^+ fractional abundances are closer to predictions from models having $\zeta \geq 10^{-14} \text{ s}^{-1}$ (see also Fig. 2). For values of ζ in this range, Figure 2 also shows that $n(H)/n(H_2)$ becomes large, so that the gas is mainly atomic. This is consistent with the inference of Neufeld et al. (2010) that the gas has a low molecular fraction. Gerin et al. (2010) detected OH^+ , H_2O^+ and H_3O^+ towards the massive star-forming region G10.6-0.4 and estimated column densities of $2.5 \times 10^{14} \text{ cm}^{-2}$, $6.0 \times 10^{13} \text{ cm}^{-2}$ and $4.0 \times 10^{13} \text{ cm}^{-2}$, respectively. The OH^+ and H_2O^+ column densities are roughly similar to those found by Neufeld et al. (2010) in W49N, which suggests that the H_3O^+ fractional abundance in G10.6-0.4 may be of the order of $\sim 10^{-9}$. Figure 2 shows that values of this order can be achieved when ζ is $\sim 2 \times 10^{-14} \text{ s}^{-1}$.

Towards Orion-KL Gupta et al. (2010) showed that despite lower OH^+ and H_2O^+ column densities than in the W49N case, a high cosmic ray ionisation rate (i.e. $\zeta \geq 1 - 2 \times 10^{-14} \text{ s}^{-1}$) is still required for reproducing these observational values. Here, we found that models with $\zeta \sim 10^{-14} \text{ s}^{-1}$ for OH^+ and models with $\zeta \geq 2 \times 10^{-14} \text{ s}^{-1}$ agree with those observational column densities. These results also seem consistent, to a first approximation, with those of Shaw et al. (2008) who showed that $\zeta > 40 \times$ the standard value (i.e. $\zeta \sim 7 \times 10^{-14} \text{ s}^{-1}$) is required to reproduce the abundances of several species in ζ Persei.

Interstellar molecular oxygen has been a target of SWAS, Odin, and - more recently - Herschel HIFI (See the talk given by P. Goldsmith at the Stormy Cosmos meeting: http://www.ipac.caltech.edu/ism2010/talks/Goldsmith_StormyCosmos2010.pdf). The Herschel results confirm and extend the earlier results. Most galactic sources show no detectable emission, suggesting that in regions of modest temperature the O_2 fractional abundance is low, with limits between a few times 10^{-9} to a few times 10^{-8} . Model results reported here show that at relatively low A_v (Fig.

2) the O_2 fractional abundance peaks at $\sim 10^{-9}$ when $\zeta \sim 1 \times 10^{-14} \text{s}^{-1}$. At larger A_v , then $X(\text{O}_2)$ is $\sim 10^{-8}$ when $\zeta \sim 1 \times 10^{-16} \text{s}^{-1}$, but falls rapidly when ζ is larger than $\sim 1 \times 10^{-14} \text{s}^{-1}$. The model results appear to be consistent with the observational data.

We consider then in particular for the extragalactic comparison, galaxies where AGN - and/or starburst - activities may have enhanced the cosmic ray ionization rates as well as, in some cases, created ULIRGs. In Bayet et al. (2009) we selected well-known galaxies, such as Arp 220 or M 82 as examples of sources with active nuclei, and where therefore the cosmic ray ionization rate may be enhanced. Arp 220 is the prototypical ultraluminous galaxy while M82 is the prototypical starburst. Recently (van der Tak et al. 2008) H_3O^+ has been discovered in these two regions and its fractional abundance has been estimated to be $\sim 2\text{--}10 \times 10^{-9}$. These authors found that observations of M 82 are matched by a high- ζ PDR, i.e., an evolved starburst while X-ray models are best at reproducing the observations of Arp 220. In fact, our models indicate that one can obtain high abundance of this ion at low (i.e. in a PDR) as well as high (i.e. dense star forming gas) extinction as long as the ζ is $\sim 10^{-13} \text{s}^{-1}$ and the metallicity is solar. At high extinction, which could represent the nuclear part of the galaxy, the abundance is higher, providing possibly a better match for the observations. We note here that we are not attempting to model Arp 220 that, since as van der Tak et al. (2008) pointed out, it has a quite unusual geometry.

Another interesting object which has been recently studied in molecular emission is Mrk 231, a ULIRG. A high resolution SPIRE FTS spectrum reveals the presence of ions such as OH^+ , CH^+ and H_2O^+ (van der Werf et al. 2010). While abundances are not derived, we can use our Table 2 to determine what type of model is able to produce high fractional abundances ($\geq 10^{-10}$) of these three ions. We find that the only regime is an environment with low metallicity (0.1 solar), very high cosmic ray ionisation rates ($\geq 10^{-16} \text{s}^{-1}$) and low visual extinction. van der Werf et al. (2010) explained the high abundances of these ions by involving XDR-chemistry. We find that, in agreement with Papadopoulos (2010), determining the origin of molecular emission from ULIRGs such as Mrk 231 is not trivial when both sources of energy (CR and X-rays) are present.

Finally, our results are necessarily indicative rather than specific in that we do not estimate molecular line intensities. Our study was motivated by the recent investigation of filaments around the central galaxies of clusters of galaxies by Bayet et al. (2010) and by the considerations of the effects of high cosmic ray ionization rates in ULIRGs by Papadopoulos (2010) as well as recent Herschel results. We find that several species, many detected in extragalactic environments, are in fact tracers of very high ionization fractions.

The general conclusions that we can draw from this study are as follows:

- The dense gas kinetic temperature in galaxies with high cosmic ray ionisation rates is elevated above Milky Way values. It reaches values $\geq 3000 \text{ K}$ for ionisation rates of about 10^{-12}s^{-1} ;
- many potential molecular tracers can be identified for dense gas in external galaxies in which the cosmic ray ioni-

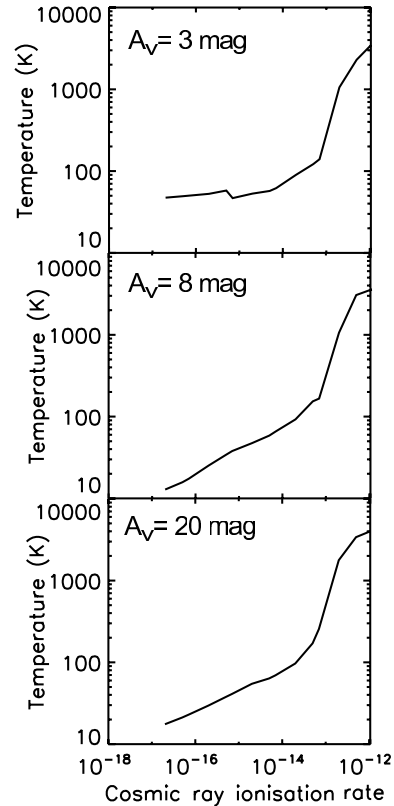


Figure 1. Temperature (in K) as a function of ζ (in s^{-1}) for $A_v = 3 \text{ mag}$ (top), 8 mag (middle) and 20 mag (bottom). See the text in Sect. 4.

sation rates are enhanced, even up to rates as large as 10^{-13}s^{-1} ;

- for galaxies with ionisation rates as large as 10^{-12}s^{-1} , gas of number density of 10^4 cm^{-3} is largely neutral and atomic, with a minor component of ions. Potential tracers of such gas are rare, but include molecular tracers OH and OH^+ and atomic tracers C and C^+ ;
- Model results for the abundances of various molecular ions detected recently in the Milky Way and in external galaxies appear to be reasonably consistent with an origin in regions of enhanced cosmic ray flux;
- if CRDRs are also regions of intense radiation fields, then translucent regions are chemically poor relative to regions that are more optically thick;
- for regions with $A_v \gtrsim 8 \text{ mags}$, the chemistry appears to be independent of depth;
- the non-linear dependence of chemistry on metallicity may allow determinations of metallicity through molecular observations.

Table 1. Model parameters (see text in Sect. 3).

Gas Density		10^4 cm^{-3}
Cosmic ray ionisation rate ζ		$5 \times 10^{-11} - 2 \times 10^{-17} \text{ s}^{-1}$
Metallicity		0.1, 1 and $4 z_{\odot}$
Gas:dust mass ratio ^a		100
H ₂ formation rate ^a	$3 \times 10^{-18} \sqrt{T} \exp(\frac{-T}{1000}) n(\text{H}) n_{\text{H}}$	$\text{cm}^{-3} \text{s}^{-1}$
C/H ^a		1.42×10^{-4}
O/H ^a		3.20×10^{-4}
S/H ^a		1.43×10^{-6}
N/H ^a		6.50×10^{-5}
Mg/H ^a		5.10×10^{-6}
He/H ^a		7.50×10^{-2}
Si/H ^a		8.21×10^{-7}
Fe/H ^a		3.60×10^{-7}
Cl/H ^a		1.10×10^{-7}
Na/H ^a		8.84×10^{-7}
Ca/H ^a		5.72×10^{-10}
Grain size		0.1 μm
Grain albedo		0.7
External FUV radiation intensity		1000 Habing ^b
A _v maximum		20 mag
Microturbulence velocity		1.5 kms^{-1}

^a : $z = 1 = z_{\odot}$ corresponds to solar values of the initial elemental abundance ratios while $z = 1/10 z_{\odot}$ means that the solar values of the initial elemental abundance ratios have been all divided by the same factor (of 10 in this example). The initial elemental abundance ratios are from Sembach & Savage (1996); Sofia et al. (1997); Meyer et al. (1998); Snow et al. (2002); Knauth et al. (2003). Similar assumptions are supposed for the H₂ formation rate coefficient and the dust:gas mass ratio; ^b: The unit of the standard Interstellar Radiation Field (ISRF) intensity is a mean intensity of $1.6 \times 10^{-3} \text{ erg cm}^{-2} \text{ s}^{-1}$ integrated over 912-2400 angstroms (Habing 1968).

Table 2. Fractional abundances ($n(X)/n_H$) of species X (see col. 1), where n_H is the total number of hydrogen atoms, for various metallicities and as a function of high cosmic ray ionisation rate ($\zeta = 1 \times 10^{-13} \text{s}^{-1}$) and lower cosmic ray ionisation rate ($\zeta = 1 \times 10^{-16} \text{s}^{-1}$). The fractional abundances are given as a(b) which represents $a \times 10^b$. The values listed are those obtained for opacities of $A_v = 3 \text{ mag}$ and $A_v = 20 \text{ mag}$ (see text in Sect. 4).

$\zeta \text{ (s}^{-1}\text{)}$ metallicity (z_\odot)	$A_v=3 \text{ mag}$						$A_v=20 \text{ mag}$					
	10^{-13}	10^{-13}	10^{-13}	10^{-16}	10^{-16}	10^{-16}	10^{-13}	10^{-13}	10^{-13}	10^{-16}	10^{-16}	10^{-16}
	0.1	1	4	0.1	1	4	0.1	1	4	0.1	1	4
Molecule												
H ₂	2.69(-3)	3.35(-1)	4.50(-1)	1.96(-2)	4.99(-1)	4.99(-1)	4.94(-1)	3.38(-1)	4.53(-1)	4.95(-1)	4.99(-1)	4.99(-1)
OH	1.11(-7)	1.19(-6)	4.26(-7)	8.75(-8)	5.66(-9)	3.08(-9)	7.20(-8)	3.63(-6)	6.61(-7)	1.37(-8)	7.53(-8)	3.82(-8)
H ₂ O	2.64(-10)	1.75(-7)	9.36(-8)	8.06(-10)	1.64(-9)	1.44(-9)	2.55(-8)	6.12(-7)	1.65(-7)	2.80(-9)	1.94(-6)	5.75(-6)
H ₂ O ⁺	2.03(-10)	4.25(-9)	1.34(-9)	1.96(-9)	1.53(-12)	1.37(-12)	2.41(-12)	7.36(-9)	1.78(-9)	2.93(-12)	1.85(-12)	2.69(-12)
C ⁺	9.43(-6)	9.95(-5)	3.59(-4)	9.91(-6)	3.14(-6)	4.03(-6)	8.18(-7)	5.74(-5)	3.18(-4)	9.94(-7)	1.66(-8)	5.03(-9)
C	4.76(-6)	3.06(-5)	1.68(-4)	4.28(-6)	8.49(-5)	1.33(-4)	1.08(-5)	1.62(-5)	1.24(-4)	1.27(-5)	6.85(-7)	9.11(-7)
CO	7.16(-9)	1.19(-5)	4.07(-5)	7.27(-9)	5.40(-5)	4.32(-4)	2.59(-6)	6.84(-5)	1.26(-4)	4.99(-7)	1.41(-4)	5.63(-4)
CH ⁺	3.82(-10)	6.37(-12)	3.29(-11)	2.54(-10)	5.50(-13)	2.62(-13)	5.03(-13)	5.98(-12)	3.14(-11)	5.13(-13)	8.94(-15)	4.67(-15)
CH	9.60(-10)	1.54(-9)	1.87(-8)	4.97(-11)	1.40(-9)	1.01(-9)	3.30(-9)	1.16(-9)	2.35(-8)	5.88(-10)	3.34(-10)	2.77(-11)
CO ⁺	8.12(-13)	9.55(-11)	1.19(-10)	6.64(-13)	1.86(-14)	2.93(-14)	6.04(-14)	1.83(-10)	1.75(-10)	1.18(-14)	4.97(-14)	7.49(-14)
C ₂ H	5.74(-16)	2.87(-11)	1.15(-9)	8.30(-16)	2.69(-10)	2.09(-10)	7.28(-10)	4.73(-11)	1.67(-9)	3.15(-11)	2.12(-12)	8.35(-14)
NH ₃	9.31(-17)	3.91(-13)	1.01(-12)	2.03(-16)	1.71(-13)	9.29(-14)	1.09(-10)	4.27(-12)	2.78(-12)	7.18(-14)	7.93(-9)	4.27(-9)
CS	2.98(-17)	1.53(-12)	3.41(-10)	1.55(-17)	5.20(-11)	1.13(-10)	2.16(-9)	7.01(-12)	1.63(-9)	1.39(-12)	3.55(-7)	1.37(-6)
SO	1.68(-16)	1.02(-12)	3.31(-12)	1.80(-16)	2.60(-12)	2.39(-11)	4.21(-12)	1.27(-11)	7.34(-12)	1.85(-14)	4.70(-8)	1.15(-7)
H ₂ CS	7.17(-24)	1.04(-16)	6.39(-15)	1.45(-23)	8.40(-14)	9.56(-14)	3.77(-12)	5.64(-16)	1.48(-14)	8.14(-15)	7.68(-11)	3.06(-11)
H ₂ S	2.00(-18)	1.19(-15)	1.15(-14)	5.74(-19)	2.09(-14)	8.42(-14)	3.86(-14)	1.67(-15)	1.53(-14)	1.34(-15)	1.20(-11)	1.86(-11)
H ₃ O ⁺	1.90(-13)	1.89(-9)	5.51(-10)	1.53(-11)	2.45(-11)	6.90(-12)	1.27(-10)	6.79(-9)	9.29(-10)	1.24(-10)	8.97(-11)	7.61(-11)
HCO ⁺	1.73(-13)	6.76(-10)	7.57(-10)	4.77(-13)	2.79(-11)	2.02(-11)	5.26(-11)	3.73(-9)	1.83(-9)	1.05(-11)	1.64(-10)	1.16(-10)
CN	6.21(-12)	6.16(-10)	8.10(-9)	3.47(-13)	2.23(-9)	1.82(-9)	4.55(-9)	1.20(-9)	1.06(-8)	2.42(-10)	7.26(-9)	3.28(-9)
HCN	6.85(-14)	1.88(-11)	6.25(-10)	3.09(-15)	2.42(-10)	7.91(-10)	1.06(-10)	9.07(-11)	1.59(-9)	2.07(-12)	2.57(-9)	8.64(-9)
HNC	6.97(-18)	5.15(-11)	3.09(-10)	7.68(-17)	1.82(-10)	5.54(-10)	3.36(-10)	2.28(-10)	1.89(-10)	2.31(-12)	1.87(-9)	2.13(-9)
OH ⁺	2.52(-8)	4.42(-9)	1.64(-9)	3.77(-8)	9.93(-13)	9.41(-13)	1.08(-12)	5.34(-9)	1.92(-9)	1.78(-12)	1.12(-12)	1.68(-12)
HOC ⁺	8.76(-14)	5.39(-11)	7.43(-11)	1.46(-13)	1.80(-14)	2.49(-14)	5.95(-14)	1.30(-10)	1.28(-10)	7.98(-15)	1.10(-13)	1.12(-13)
H ₂ CO	3.53(-19)	7.21(-14)	1.23(-12)	1.709(-18)	4.65(-12)	2.48(-12)	1.43(-10)	2.08(-13)	1.87(-12)	9.33(-13)	1.22(-11)	1.32(-12)

ACKNOWLEDGMENTS

EB acknowledges financial support from STFC. We thank the referee for constructive comments that have improved the original version of the paper.

REFERENCES

- Aalto S., 2008, *Ap&SS*, 313, 273
- Acciari V. A., Aliu E., Arlen T., Aune T., Bautista M., Beilicke M., VERITAS Collaboration 2009, *Nature*, 462, 770
- Acerro F., Aharonian F., Akhperjanian A. G., Anton G., Barres de Almeida U., Bazer-Bachi A. R., Becherini Y., Behera B., 2009, *Science*, 326, 1080
- Bayet E., Aladro R., Martín S., Viti S., Martín-Pintado J., 2009, *ApJ*, 707, 126
- Bayet E., Gerin M., Phillips T. G., Contursi A., 2006, *A&A*, 460, 467
- Bayet E., Hartquist T. W., Viti S., Williams D. A., Bell T. A., 2010, *A&A*, 521, A16+
- Bayet E., Viti S., Williams D. A., Rawlings J. M. C., 2008, *ApJ*, 676, 978
- Bayet E., Viti S., Williams D. A., Rawlings J. M. C., Bell T., 2009, *ApJ*, 696, 1466
- Bell T. A., Roueff E., Viti S., Williams D. A., 2006, *MNRAS*, 371, 1865
- Bell T. A., Viti S., Williams D. A., Crawford I. A., Price R. J., 2005, *MNRAS*, 357, 961
- Black J. H., Dalgarno A., 1977, *ApJS*, 34, 405
- Boger G. I., Sternberg A., 2006, *ApJ*, 645, 314
- de Jong T., Boland W., Dalgarno A., 1980, *A&A*, 91, 68
- Ercolano B., Barlow M. J., Storey P. J., 2005, *MNRAS*, 362, 1038
- Ferland G. J., Korista K. T., Verner D. A., Ferguson J. W., Kingdon J. B., Verner E. M., 1998, *PASP*, 110, 761
- Gerin M., de Luca M., Black J., Goicoechea J. R., Herbst E., 2010, *A&A*, 518, L110+
- Gupta H., Rimmer P., Pearson J. C., Yu S., Herbst E., Harada N., Bergin E. A., Neufeld D. A., Melnick G. J., Bachiller R., Baechtold W. a., 2010, *A&A*, 521, L47+
- Habing H. J., 1968, *Bul. of the Astron. Inst. of the Netherlands*, 19, 421
- Hartquist T. W., Black J. H., Dalgarno A., 1978, *MNRAS*, 185, 643
- Hartquist T. W., Doyle H. T., Dalgarno A., 1978, *A&A*, 68, 65
- Indriolo N., Fields B. D., McCall B. J., 2009, *ApJ*, 694, 257
- Indriolo N., Geballe T. R., Oka T., McCall B. J., 2007, *ApJ*, 671, 1736
- Knauth D. C., Andersson B.-G., McCandliss S. R., Moos H. W., 2003, *ApJ Letter*, 596, L51
- Lee H., Herbst E., Pineau des Forets G., Roueff E., Le Bourlot J., 1996, *A&A*, 311, 690
- Lepp S., Tiné S., 1998, *The Molecular Astrophysics of Stars and Galaxies*, edited by Thomas W. Hartquist and David A. Williams. Clarendon Press, Oxford, 1998., p.489, 4, 489
- Meijerink R., Spaans M., 2005, *A&A*, 436, 397
- Meijerink R., Spaans M., Israel F. P., 2006, *ApJ Letter*, 650, L103
- Meyer D. M., Jura M., Cardelli J. A., 1998, *ApJ*, 493, 222
- Neufeld D. A., Goicoechea J. R., Sonnentrucker P., Black J. H., Pearson J., Yu S., Phillips T. G. a., 2010, *A&A*, 521, L10+
- Papadopoulos P. P., 2010, *ApJ*, 720, 226
- Papadopoulos P. P., Thi W.-F., Miniati F., Viti S., 2010, *MNRAS*, submitted
- Röllig M., Abel N. P., Bell T., Bensch F., Black J., Ferland G. J., Jonkheid B., Kamp I., Kaufman M. J., Le Bourlot J., Le Petit F., etc., 2007, *A&A*, 467, 187
- Schöier F. L., van der Tak F. F. S., van Dishoeck E. F., Black J. H., 2005, *A&A*, 432, 369
- Sembach K. R., Savage B. D., 1996, *ApJ*, 457, 211
- Shaw G., Ferland G. J., Srianand R., Abel N. P., van Hoof P. A. M., Stancil P. C., 2008, *ApJ*, 675, 405
- Snow T. P., Rachford B. L., Figoski L., 2002, *ApJ*, 573, 662
- Sofia U. J., Cardelli J. A., Guerin K. P., Meyer D. M., 1997, *ApJ Letter*, 482, L105+
- Spaans M., Meijerink R., 2005, *Ap&SS*, 295, 239
- Suchkov A., Allen R. J., Heckman T. M., 1993, *ApJ*, 413, 542
- van der Tak F. F. S., Aalto S., Meijerink R., 2008, *A&A*, 477, L5
- van der Werf P. P., Isaak K. G., Meijerink R., Spaans M., Rykala A., Fulton T., 2010, *A&A*, 518, L42+
- Zaritsky D., Kennicutt R. C., Huchra J. P., 1994, *ApJ*, 420, 87

This paper has been typeset from a $\text{\TeX}/\text{\LaTeX}$ file prepared by the author.

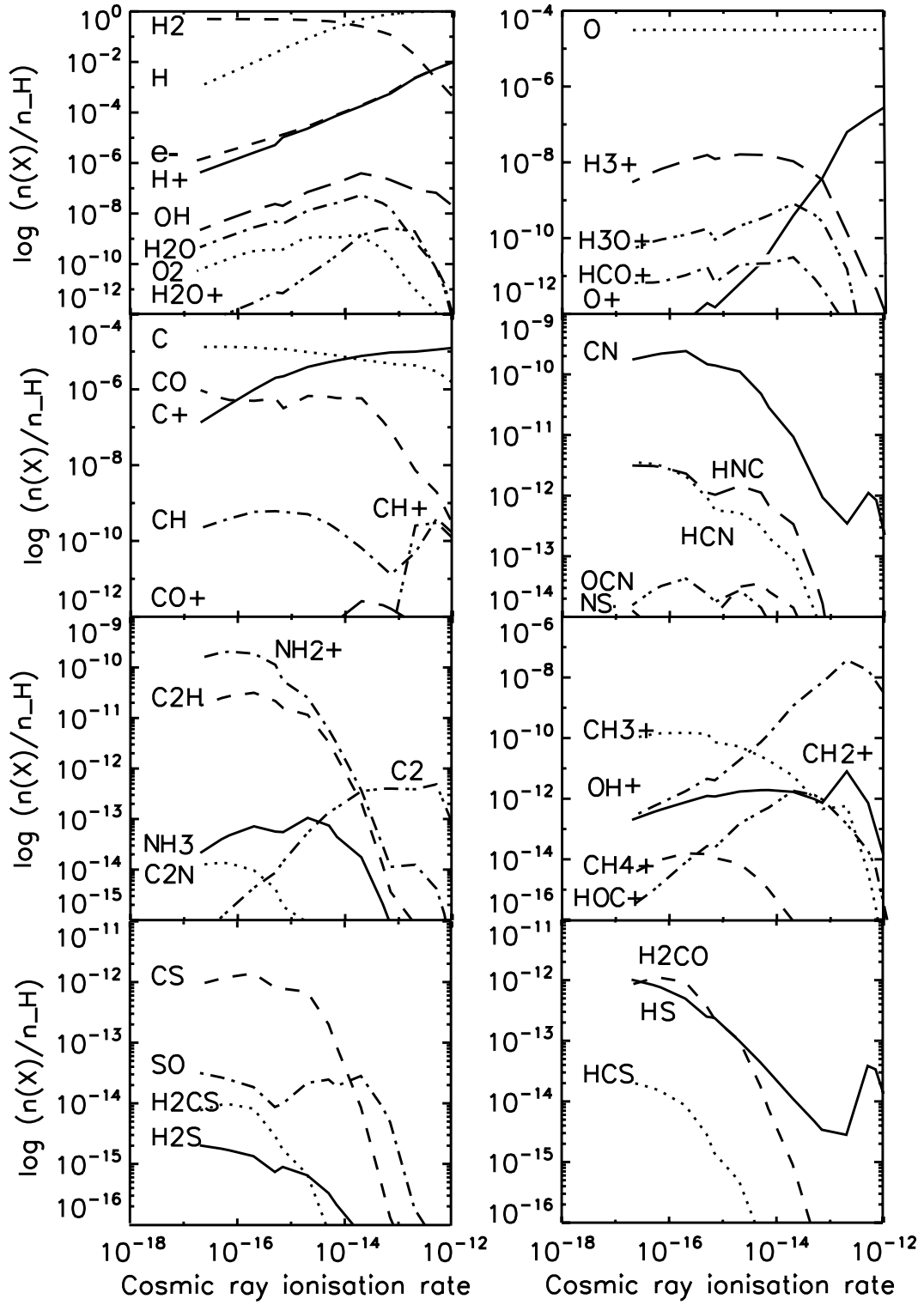


Figure 2. Fractional abundances ($n(X)/n_H$) of species X in logarithmic scale where n_H is the total number of hydrogen atoms, obtained for the models with a metallicity of $0.1 z_\odot$ for an A_V of 3 mag as functions of cosmic ray ionisation rate (ζ) in s^{-1} (see text in Sect. 4).

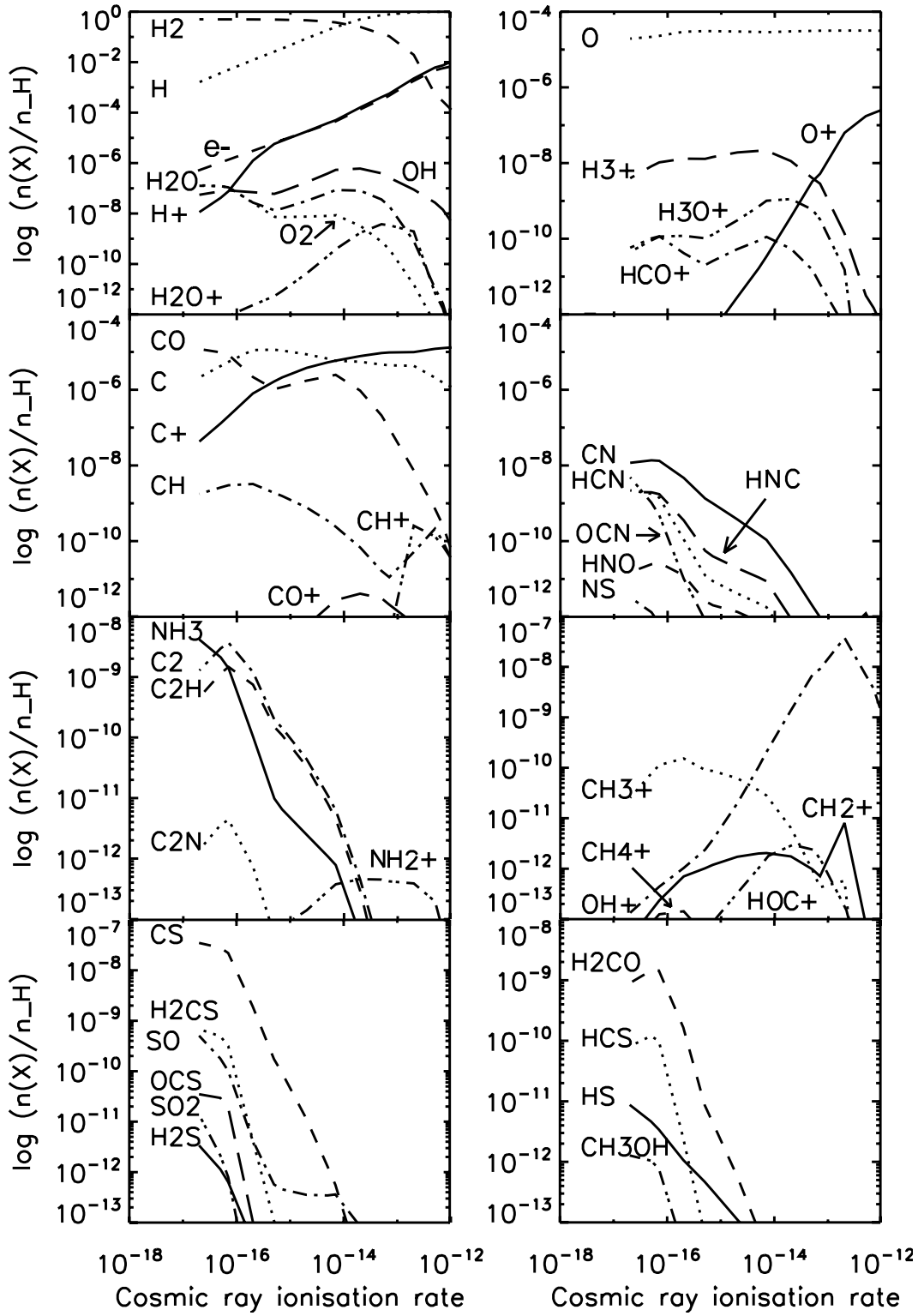


Figure 3. Fractional abundances of species X obtained for the models with a metallicity of $0.1 z_{\odot}$ for an A_V of 8 mag (see text in Sect. 4 and the caption of Fig. 2).

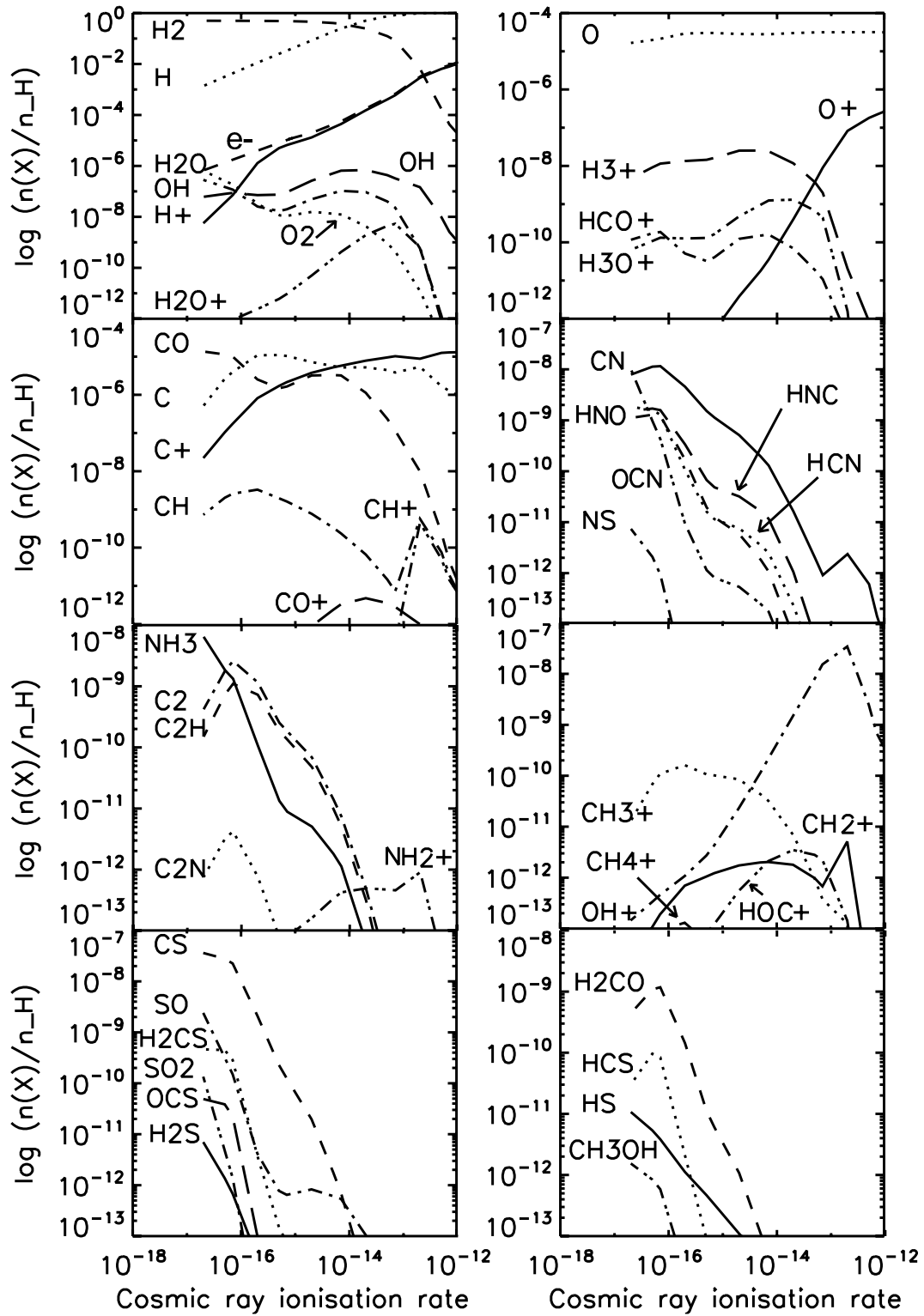


Figure 4. Fractional abundances of species X obtained for the models with a metallicity of $0.1 z_{\odot}$ for an A_V of 20 mag (see text in Sect. 4 and the caption of Fig. 2).